Experimental investigation of the effect of floating motion on the wake recovery of a floating wind turbine using particle tracking velocimetry

Journal of Physics: Conference Series **3224** (2026) 082015 doi:10.1088/1742-6596/3224/8/082015

Experimental investigation of the effect of floating motion on the wake recovery of a floating wind turbine using particle tracking velocimetry

Federico Taruffi[1], Carlos Miron Vidal[1], Giulia Pomaranzi[2] and Axelle Viré[1]

[1]Faculty of Aerospace Engineering, Delft University of Technology, Delft, the Netherlands

[2]Department of Mechanical Engineering, Politecnico di Milano, Milano, Italy

E-mail: F.Taruffi@tudelft.nl

Abstract. Floating offshore wind turbines experience platform motions that can modify wake development and, consequently, wind farm performance. In this study, the effects of imposed platform motion on wake recovery are investigated experimentally using hybrid wind tunnel tests combined with 3D-PTV technique. Measurements are performed under low-turbulence inflow conditions, enabling isolation of motion-induced effects on the turbine wake. The wake is characterised from the near- to the mid-wake region for static and moving platform configurations, considering surge and pitch motions over a range of reduced frequencies. The results show that platform motions can enhance wake recovery by accelerating the transition towards the far wake, with a dependence on motion frequency and type. Motions representative of floater rigid-body natural modes improve wake recovery, particularly for surge motion. In contrast, higher reduced-frequency motions, representative of wave-induced excitation, exhibit a much weaker influence on wake development, yielding wake characteristics close to the static configuration.

1. Introduction

Floating offshore wind turbines (FOWTs) are a key technology for exploiting the vast wind energy resources available in deep waters, where bottom-fixed foundations are not feasible. Following the successful deployment of pilot projects, floating wind is expected to expand rapidly in the coming years, with commercial-scale farms reaching the gigawatt level.

Unlike bottom-fixed turbines, floating support structures introduce platform motions in six degrees of freedom, driven by the combined action of wind, waves and currents. These motions influence both the aerodynamic performance of the turbine and the characteristics of its downstream wake. Since wake interactions strongly affect the power production and loading of downstream turbines, understanding how platform motions modify wake recovery is fundamental for predicting farm-level performance and optimising the layout of floating wind farms.

Several experimental and numerical studies have shown that platform motions can alter wake characteristics, including velocity deficit, turbulence intensity, and wake development. In some cases, these effects have been associated with accelerated wake recovery and a potential

improvement in overall farm efficiency. However, isolating and quantifying the role of platform motions remains challenging, primarily due to their interaction with ambient inflow turbulence, which itself plays a dominant role in wake recovery. As a result, previous studies have reported inconsistent findings. Early wind tunnel experiments by [1] indicated neutral or even adverse effects of platform motion, in agreement with subsequent numerical investigations [2]. Field-scale lidar measurements by [3] further suggest that, under realistic atmospheric conditions, ambient turbulence largely governs wake behaviour, with only negligible additional recovery attributable to floating motions. These observations highlight the need to decouple platform-motion effects from inflow turbulence in order to achieve a more fundamental understanding of floating wind turbine wake dynamics.

To this end, more recent studies have employed wind tunnel experiments under nearly uniform inflow conditions ($TI \leq 2\%$). [4] investigated a 2.4m diameter scale turbine subjected to harmonic platform motions at reduced frequencies [0.3, 0.6, 1.2]. Wake-deficit measurements at $3D$ and $5D$ downstream showed no appreciable change in recovery relative to the static case. However, the increase in turbulence intensity at the wake centre suggested a shift of the mixing layer toward the wake core, potentially improving wake recovery farther downstream than was measured. Using a similar experimental approach with a smaller rotor ($D = 0.6$m), [5] systematically examined wake recovery under imposed surge and pitch motions across reduced frequencies from 0 to 0.97. In contrast to the findings of [4], their results indicated that surge and pitch motions can significantly enhance wake recovery (up to 25% compared to the fixed case) for reduced frequencies above 0.3, suggesting an earlier merging of the wake under imposed motion.

The present work contributes to resolving these inconsistencies by experimentally characterising the near- to mid-wake region (from $1D$ to $5D$ downstream) of a moving scale rotor in a wind tunnel under smooth inflow conditions, thereby isolating the effects of platform motion on wake dynamics. Three-dimensional particle tracking velocimetry (3D-PTV) using helium-filled soap bubbles (HFSB) is employed as a volumetric, non-intrusive measurement technique, enabling detailed spatial reconstruction over large continuous volumes. This results in an extensive experimental dataset, which is openly available to the scientific community at [6]. The primary objective of this study is to quantify the influence of surge and pitch motions on wake recovery across a wide range of reduced frequencies, spanning those associated with platform rigid-body modes and extending to higher frequencies representative of wave-induced motions, beyond the range explored in previous experimental investigations.

2. Experimental setup

The experimental setup consists of a wind turbine scale model mounted on a hexapod robot. The 1.2m diameter physical rotor is a 1 : 148 model version of the DTU 10MW operating with a velocity scale of 1 : 3, scaled with a performance-scale approach to match the thrust force, and with a modified airfoil (SD7032) suitable for low-Reynolds applications such as the present one, where the operating Reynolds number is about 50k. The turbine is mounted on a six-degrees-of-freedom parallel kinematics hexapod robot to actuate the floating motions. A detailed description of the hybrid setup can be found in [7]. The tests are performed in TU Delft's open jet facility, a closed-circuit open-section wind tunnel with a 3m nozzle opening on a 6m wide, 6.5m high, and 13.5m long test section. The flow is uniform and laminar with a turbulence intensity spanning from 0.5% at 1m from the nozzle to an evenly spread 2% at 6m inside the measurement region. While this increase in turbulence intensity is unavoidable due to the inherent shear-layer development at the exit of the wind-tunnel nozzle [8], measurements

of the undisturbed flow allow for quantifying its influence within the measurement region.

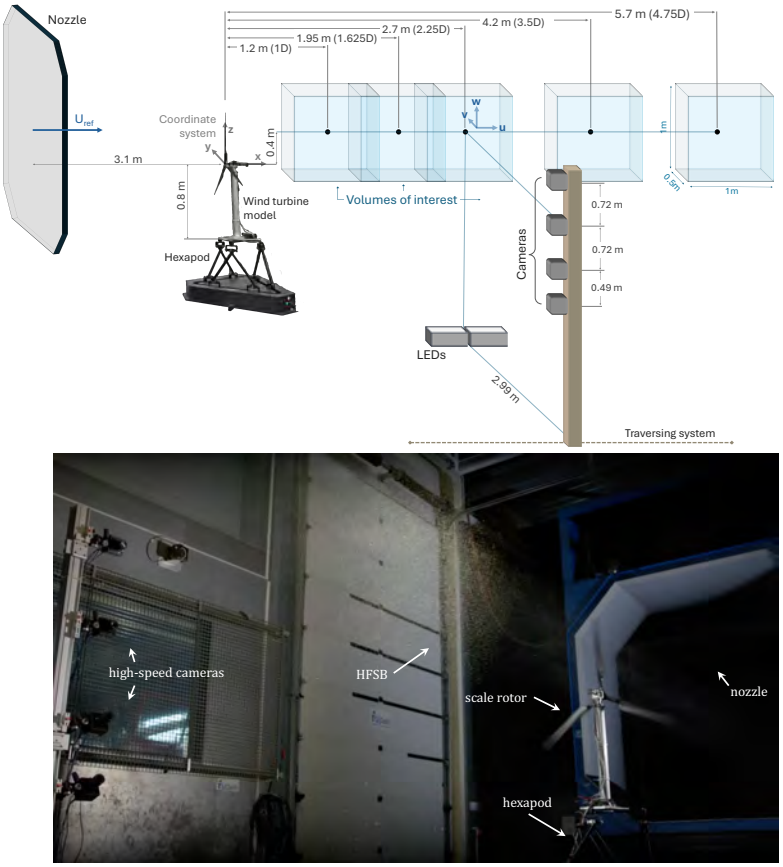

Figure 1. Sketch of the setup (top) and snapshot of a test (bottom).

The wake velocity is measured using 3D-PTV with HFSB as tracers [9]. This technique shares similarities with tomographic PIV in terms of optical arrangement and multi-camera acquisition. However, rather than relying on a voxel-based reconstruction and spatial cross-correlation, it is purely a particle-based technique. Individual particles are identified based on peak intensity in the images and subsequently triangulated to obtain their three-dimensional positions. The particle size is about $0.3 - 0.4$mm and their relaxation time is about $0.01 - 0.04$ms, giving a frequency response in the order of 10kHz. Particle trajectories are reconstructed using iterative particle reconstruction combined with time-resolved tracking, allowing direct computation of Lagrangian velocities and the capture of complex, unsteady wake dynamics. The method used to reconstruct the particle field velocity is the vortex-in-cell plus method [10], due to its high spatial resolution and its ability to accurately determine turbulent structures.

Four high-speed cameras, mounted on a vertical pole and placed perpendicular to the flow, record images at 400Hz for a duration of 10s. Two LEDs aligned in the streamwise direction illuminate the tracers from below. This arrangement allows for a field of view of approximately 1m in streamwise, 0.5m in lateral (centred with the rotor), and 1m in vertical direction, capturing the upper half of the rotor and extending by approximately 20% beyond it upwards and downwards. Five volumes are recorded separately by moving the measurement downstream and subsequently merging the particle fields. LaVision DaVis software is used for the postprocessing.

The wind turbine model is operated at rated conditions, with a wind speed of 4m/s and a rotor speed of 480rpm (the tip-speed ratio is 7.5), generating a measured thrust force of 8.8N, corresponding to a thrust coefficient of 0.79. Imposed platform motions are surge and pitch sinusoids at reduced frequencies $St = fD/U$ of 0.6 and 1.5 - corresponding to model scale frequencies 2Hz and 5Hz respectively - and amplitudes calculated to obtain a normalised velocity variation at the hub $\Delta V/U$ of 0.1 (which correspond to: velocity variation $\Delta V = 0.4$m/s; surge amplitudes of 31.8mm at $St = 0.6$ and 12.7mm at $St = 1.5$; pitch amplitudes of 1.57deg at $St = 0.6$ and 0.63deg at $St = 1.5$, considering a pitch arm of 1.16m; expected amplitudes of quasi-steady thrust and thrust coefficient variation of approximately 1N and 0.09 [7]). The reduced frequency of 0.6 is selected to match the pitch natural frequency for a 10MW semi-submersible floating turbine and used for both pitch and surge cases to highlight any difference due to the motion type. This is also the reduced frequency that previous studies highlight as the most important for wake recovery purposes [4]. On the other hand, we also explore reduced frequency typical of wave-induced motions, which should lead to $St = 1.5$ [5]. Moreover, those two frequencies allow for the investigation of motions both inside and outside the quasi-steady behaviour region, characterised by reduced frequencies below 1.2 [7]. The normalised velocity variation of 0.1 is chosen based on [7] and lies on the higher end of the considered values to accentuate the motion effects on the wake. Although larger than what is expected from wave-induced motions, the same value is used with both reduced frequencies to keep the thrust variation constant across cases.

Measurements counted five volumes, located downstream at distances spanning from 0.6D to 5.1D (covering seamlessly from 0.6D to 2.6D, from 3.1D to 3.9D, and from 4.3 to 5.1D). Here, 5.1D corresponds to the furthest downstream location for which accurate measurements were achievable. Measurements at some intermediate distances were omitted to focus continuously on the near-wake region where more dynamics are expected, while also having measurements in the mid-/far-regions. The convergence of the measurements is assessed using a running average of the velocity components, and the acquisition time of 10s, which is limited by the high-speed cameras' buffer, is found to be sufficient to achieve a statistically converged mean. The velocity measurement uncertainty is quantified to be below 3% over the entire domain.

3. Results

3.1. Streamwise velocity

Time-averaged mid-plane ($y = 0$) normalized streamwise velocity fields (U/U_∞) for the static configuration and the imposed motion cases are shown in Fig. 2. For imposed surge motion at low reduced frequency ($St = 0.6$), differences with respect to the static case are negligible in the very near wake ($x \leq 1.5D$). Further downstream, however, the two fields diverge, with the moving-platform case exhibiting a systematically faster wake recovery, characterised by higher streamwise velocity levels within the wake compared to the static configuration.

In contrast, the high reduced-frequency surge case ($St = 1.5$) shows limited deviations from the static wake over most of the domain. Only in the far-wake region ($4.3D \leq x \leq 5.1D$) does a slight increase in velocity appear within the wake core, suggesting a marginal enhancement of wake recovery under high-frequency motion. Pitch motions exhibit qualitatively similar trends. For the low reduced-frequency pitch case ($St = 0.6$), increased streamwise velocities are observed downstream of $x \approx 1.5D$ relative to the static case, indicating enhanced wake recovery. However, although recovery at $x \approx 5D$ is improved, it remains noticeably weaker than that observed for the corresponding low reduced-frequency surge motion.

At high reduced frequency ($St = 1.5$), pitch motion produces only minor deviations from the

static wake. Differences are negligible in the near wake ($x \leq 2.5D$), while further downstream the flow remains highly similar to the static configuration, with only localised and modest increases in streamwise velocity near the wake centerline.

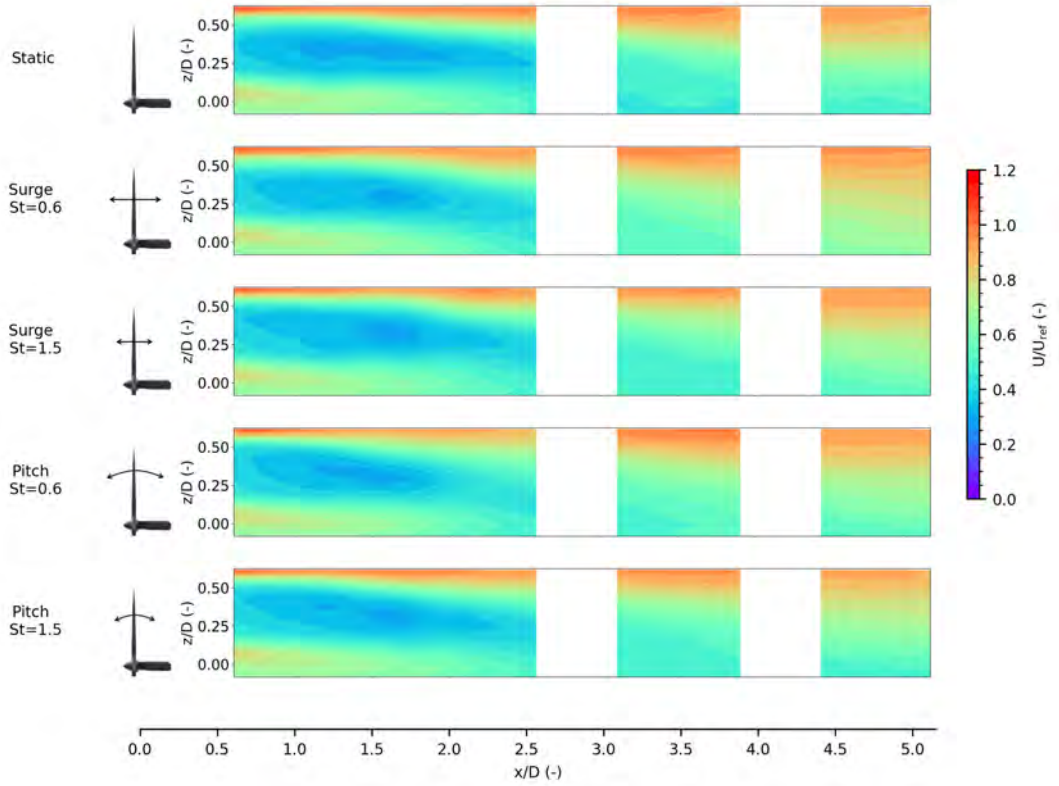

Figure 2. Time-averaged streamwise velocity extracted from the vertical plane at $y = 0$. From top to bottom: static, surge $St = 0.6$, surge $St = 1.5$, pitch $St = 0.6$, pitch $St = 1.5$.

3.1.1. Wake deficit For a more quantitative comparison, wake velocity deficit profiles are extracted at several downstream locations and shown in Fig. 3, including all motion cases. At $x = 1D$, all profiles almost collapse onto the static case, indicating that platform motion does not influence the very near wake.

At $x \approx 2.25D$, the motion cases exhibit a noticeable change in profile shape, characterised by flatter distributions compared to the static configuration. This effect is particularly pronounced for the low reduced-frequency motions, consistent with their higher turbulence levels (Fig. 5) and enhanced mixing (Fig. 6). Further downstream, at $x \approx 3.75D$, the low reduced-frequency surge case ($St = 0.6$) shows the most significant wake recovery, with an increase in streamwise velocity of approximately 20% at hub height relative to the static case. This enhancement gradually diminishes toward the blade tip. In contrast, the high reduced-frequency cases ($St = 1.5$) remain closely aligned with the static profile up to $z \approx 0.3D$, above which a slightly lower recovery is observed. In the far-wake region ($x = 5D$), the low reduced-frequency surge motion continues to be the most effective in accelerating wake recovery, displaying a clear departure from the low reduced-frequency pitch case, which instead aligns more closely with the profiles associated with high reduced-frequency motions.

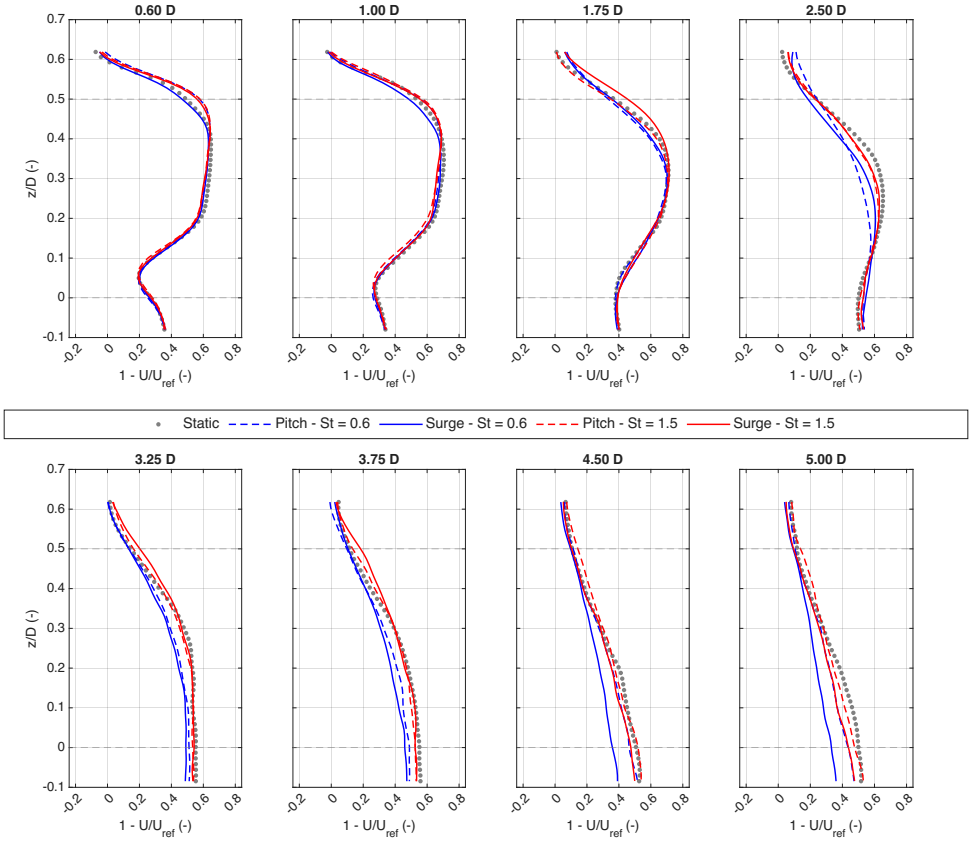

Figure 3. Wake deficit at (from left to right) 0.6D, 1D, 1.75D, 2.25D, 3.25D , 3.75D, 4.5D and 5D. Cases: static, surge and pitch cases at $St = 0.6$ and $St = 1.5$.

3.1.2. Recovery To quantify the impact of motion frequency on wake recovery, the average wind speed in the rotor area behind the turbine is computed at several downstream locations. The mean wake velocity is obtained by averaging the local velocity over the rotor-swept area using annular-area weighting. Specifically, considering the radial samples U extracted at $y = 0$ for different heights z_i (sorted from hub to tip) and defining the annular area $\Delta A_i = \pi\left(z_i^2 - z_{i-1}^2\right)$, the rotor-averaged velocity is computed as

$$\overline{U}(x) = \frac{\sum_{i=1}^{N} U(x, z_i)\,\Delta A_i}{\sum_{i=1}^{N} \Delta A_i} \tag{1}$$

and is reported normalised by the reference velocity U_{ref}, i.e. $\overline{U}/U_{\text{ref}}$. Figure 4 presents the results for the surge cases. At a reduced frequency of $St = 0.6$, surge motion leads to enhanced wake recovery compared to the static configuration, with the effect becoming more pronounced beyond $2.5D$ downstream. In contrast, for the higher-frequency case ($St = 1.5$), only minor deviations from the static wake are observed, indicating a negligible influence of surge motion on wake recovery at this frequency.

3.2. Turbulence intensity

Figure 5 reports the turbulence intensity (TI) for all cases. For the low reduced-frequency surge case ($St = 0.6$), a localised increase in TI is observed between $x \approx 1.2D$ and $2.5D$, co-located with the region of enhanced mean velocity recovery. This behaviour indicates that

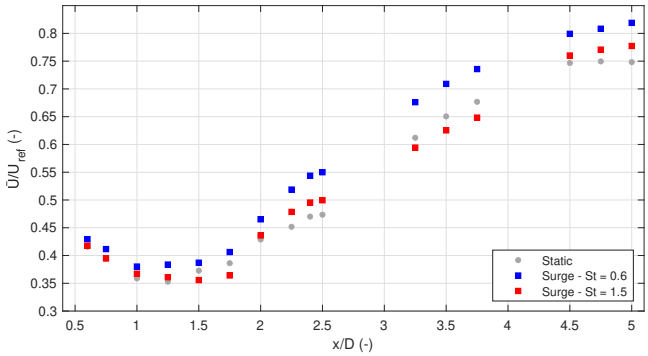

Figure 4. Wake recovery integrated over the rotor area for static and surge $St = 0.6$ and $St = 1.5$ cases.

platform-induced unsteadiness accelerates flow mixing in the near wake. Further downstream ($x \approx 3{-}4D$), TI in the surge case converges to, and subsequently drops below, the static level, indicating an earlier transition toward the far-wake regime under imposed motion. A similar trend is observed for the low reduced-frequency pitch case ($St = 0.6$). Here, enhanced near-wake turbulence arises as rotor motion increases turbulent mixing, leading to a more rapid wake development and an earlier transition to a less turbulent far wake at the downstream measurement locations. In contrast, the effects of high reduced-frequency motions ($St = 1.5$) on turbulence intensity are considerably weaker for both surge and pitch. In the near wake ($x \leq 2.5D$), a modest increase in TI of approximately 4% is observed. Although limited, this increase still contributes to an earlier wake transition further downstream, where TI levels fall slightly below those of the static case. Overall, this behaviour mirrors that observed for the low reduced-frequency cases, but with reduced magnitude, reflecting the smaller motion amplitudes associated with high reduced-frequency excitation.

3.3. Reynolds stress, vorticity and swirling strength

The Reynolds stress component $\overline{u'w'}$ provides a direct measure of vertical momentum transport and is therefore an indicator of wake mixing and recovery [11]. In particular, it represents the entrainment of high-momentum freestream fluid, predominantly from above the rotor, into the low-momentum wake. Additional localised regions of both upward and downward momentum transport are observed near the blade root, hub, nacelle, and tower. When low reduced-frequency platform motions ($St = 0.6$) are imposed, the near wake exhibits a substantially higher magnitude of $\overline{u'w'}$ compared to the static case between approximately $1D$ and $2.6D$. This increase reflects enhanced vertical mixing between the freestream and the wake induced by rotor motion, leading to elevated turbulence levels in this region. As a consequence, the wake experiences a reduced velocity deficit and an accelerated recovery of the streamwise velocity, consistent with previous studies linking increased Reynolds shear stress to faster wake recovery [11, 12]. Further downstream, the magnitude of $\overline{u'w'}$ decreases as the velocity difference between the wake and the surrounding flow diminishes, weakening the driving mechanism for turbulent mixing. In contrast, the high reduced-frequency motion cases ($St = 1.5$ for both surge and pitch) display Reynolds stress distributions that closely resemble the static configuration. Only minor variations in $\overline{u'w'}$ are observed, indicating that these motions are not sufficiently energetic to significantly modify vertical momentum transport. Consequently, wake recovery under high reduced-frequency excitation can be considered quasi-static. Overall, the Reynolds stress results demonstrate that large-amplitude, low reduced-frequency motions enhance vertical momentum transport, provid-

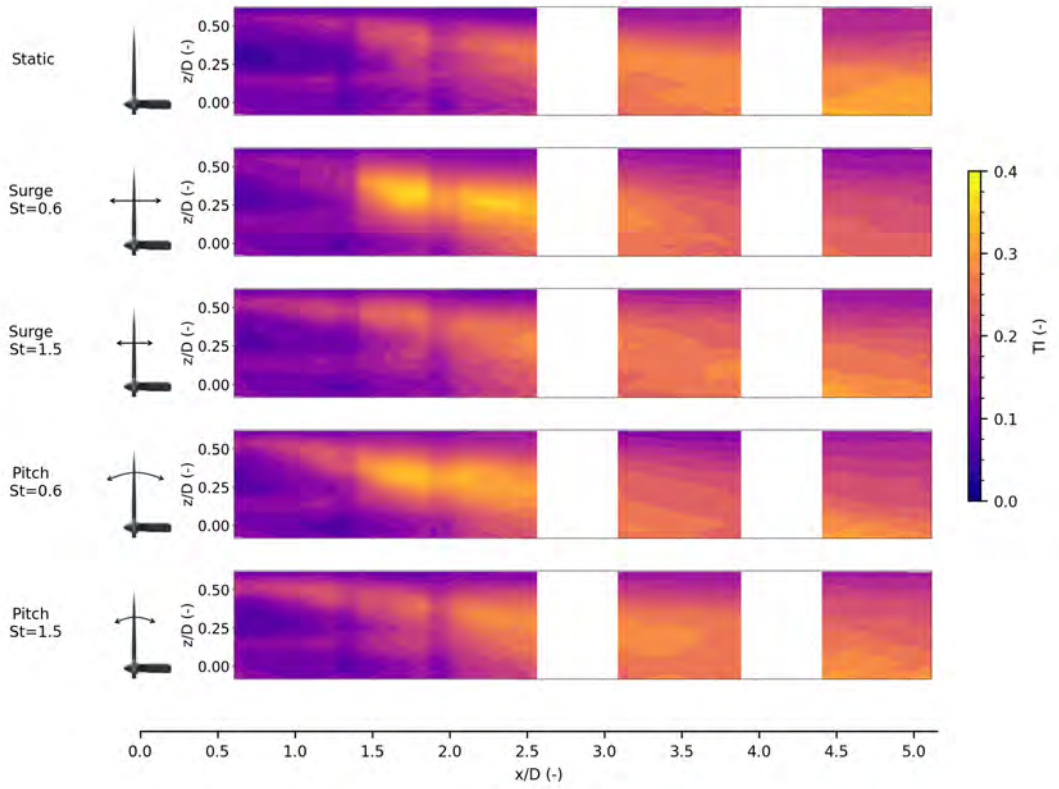

Figure 5. Turbulence intensity extracted from the vertical plane at $y = 0$. From top to bottom: static, surge $St = 0.6$, surge $St = 1.5$, pitch $St = 0.6$, pitch $St = 1.5$. Vertical bands caused by view stitching.

ing a mechanistic explanation for the previously observed increases in turbulence intensity and accelerated wake recovery.

The vorticity and swirling strength visualisations provide further insight into the evolution and stability of coherent wake structures, particularly the blade tip and root vortices. Time-averaged iso-surfaces with a threshold of 2.4 s^{-2} are shown for the first three measurement volumes only (Fig. 7), as this region contains the most relevant dynamics. The analysis focuses on surge case at $St = 0.6$, since it is the case that shows the most significant changes with respect to the static one. This imposed motion leads to a clear modification of the vortical structures compared to the static configuration. In the moving-platform case, the vortex cores appear broader and less coherent, indicating enhanced diffusion of vorticity and an earlier breakdown of coherent structures. Reduced vorticity intensity is observed closer to the rotor, suggesting that platform-induced unsteadiness accelerates the interaction and decay of the blade tip vortices. This accelerated breakdown of coherent structures is consistent with the elevated Reynolds stresses and increased vertical mixing identified in the near wake, and is consistent with the enhanced wake recovery observed under low reduced-frequency surge motion.

3.4. Discussion

Overall, the results consistently show that platform motion influences wake development primarily through its effect on turbulence generation and vertical momentum transport, with a strong dependence on motion frequency and type. Low-frequency motions ($St = 0.6$), particularly

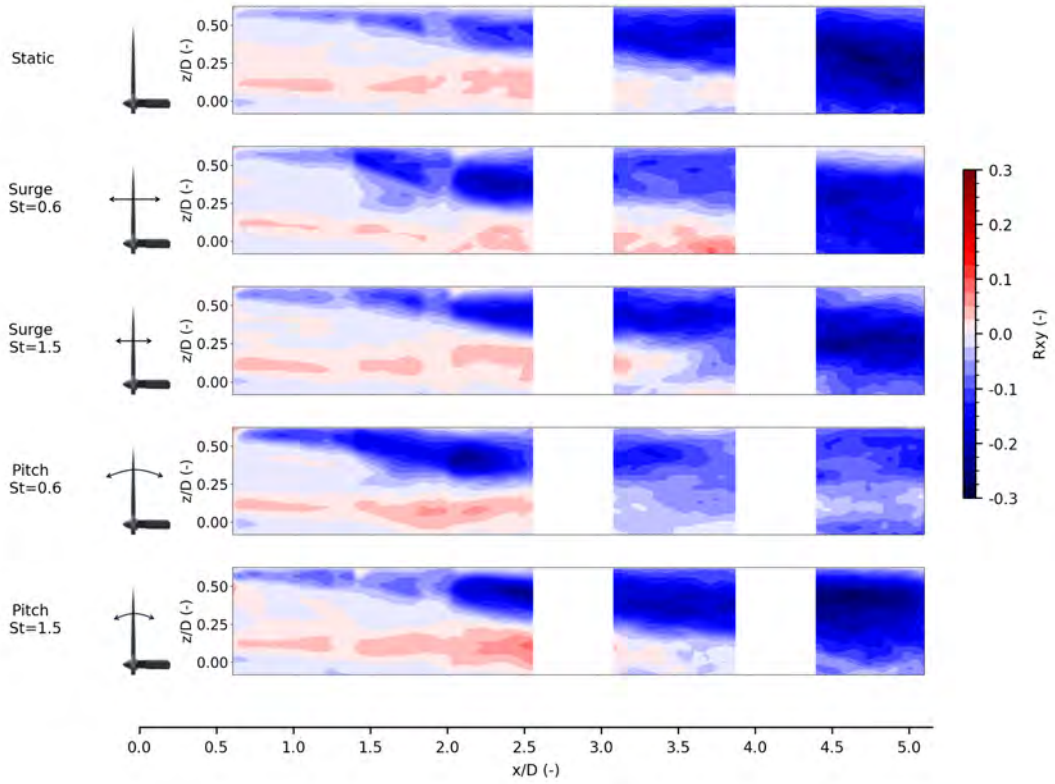

Figure 6. Reynolds stress $u'w'$ extracted from the vertical plane at $y = 0$. From top to bottom: static, surge $St = 0.6$, surge $St = 1.5$, pitch $St = 0.6$, pitch $St = 1.5$.

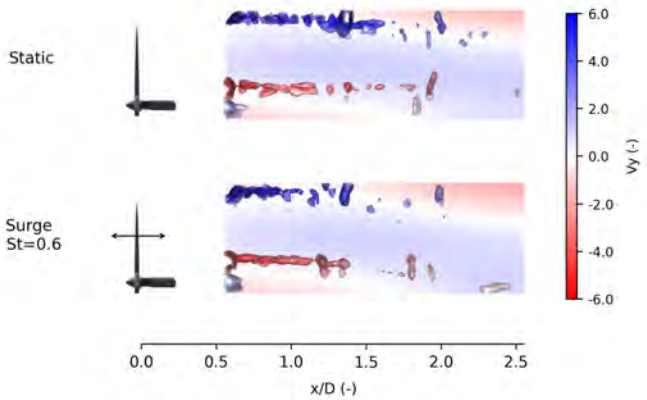

Figure 7. Swirling strength iso-surfaces coloured by vorticity, and streamwise velocity trend in the background for the vertical plane at $y = 0$ and downstream distance 0.6–2.5D. From top to bottom: static and surge $St = 0.6$.

surge, systematically enhance near-wake mixing, as evidenced by increased turbulence intensity and Reynolds stress levels between approximately $1D$ and $2.5D$. This enhanced mixing leads to a reduction in velocity deficit, accelerated breakdown of coherent vortical structures, and a

faster recovery of the mean streamwise velocity in the mid- to far-wake regions. Pitch motion at the same reduced frequency produces similar but weaker effects, resulting in a more limited enhancement of wake recovery. In contrast, high-frequency motions ($St = 1.5$) induce only modest changes to turbulence levels and Reynolds stresses, yielding wake characteristics that remain largely comparable to the static configuration. A frequency-dependent wake response has also been reported in studies where sinusoidal perturbations were artificially imposed on the turbine forcing [13], showing that different reduced frequencies can affect the wake to different extents.

4. Conclusions

The effects of platform motion on the wake recovery of a floating offshore wind turbine have been experimentally investigated through hybrid wind tunnel tests using 3D-PTV. The measurements allowed the wake development under imposed platform motion to be characterised from the near- to the mid-wake region under controlled smooth inflow conditions. Results show that platform motion can enhance wake recovery by accelerating the transition towards the far-wake regime, with a strong dependence on motion frequency and type. Motions with reduced frequencies representative of floater rigid-body modes produce a clear improvement in wake recovery, particularly for surge motion, while pitch motion exhibits a weaker effect. This enhancement is associated with increased near-wake turbulence and vertical momentum transport. In contrast, higher reduced-frequency motions, representative of wave-induced excitation, have a limited impact on wake development, producing wake characteristics close to the static configuration.

These observations suggest that enhanced wake recovery is linked to the ability of floating platform motions to introduce large-scale, energetically relevant unsteadiness in the near wake, which promotes turbulent mixing and momentum transport. Similar mechanisms relating wake recovery to turbulence production and wake dynamics have been reported in previous studies of turbine wakes and floating wind turbines [5, 11, 12]. Future work will focus on extending the present analysis to more realistic offshore atmospheric boundary layer inflow conditions in order to assess the combined effects of ambient turbulence and platform motion on floating wind turbine wakes.

Acknowledgements

Authors would like to acknowledge Andrea Sciacchitano for his guidance in preparing the experiments and Daniele Ragni for his support in post-processing the data.

References

[1] Rockel S, Camp E, Schmidt J, Peinke J, Cal R B and Hölling M 2014 Experimental study on influence of pitch motion on the wake of a floating wind turbine model *Energies* **7** 1954–1985 URL https://doi.org/10.3390/en7041954

[2] Amaral R, Houtin-Mongrolle F, von Terzi D, Laugesen K, Deglaire P and Viré A 2025 Investigating the dynamics of floating wind turbine wakes under laminar flow using large eddy simulations *Wind Energy Science Discussions* **2025** 1–43 URL https://doi.org/10.5194/wes-2025-34

[3] Angelou N, Mann J and Dubreuil-Boisclair C 2023 Revealing inflow and wake conditions of a 6mw floating turbine *Wind Energy Science Discussions* **2023** 1–35 URL https://doi.org/10.5194/wes-8-1511-2023

[4] Fontanella A, Fusetti A, Cioni S, Papi F, Muggiasca S, Persico G, Dossena V, Bianchini A and Belloli M 2025 Wake development in floating wind turbines: new insights and an open dataset from wind tunnel experiments *Wind Energy Science* **10** 1369–1387 URL https://doi.org/10.5194/wes-10-1369-2025

[5] Messmer T, Hölling M and Peinke J 2024 Enhanced recovery caused by nonlinear dynamics in the wake of a floating offshore wind turbine *Journal of Fluid Mechanics* **984** A66 URL https://doi.org/10.1017/jfm.2024.175

[6] Taruffi F and Pomaranzi G 2026 Wind tunnel wake measurements of a floating wind turbine with particle tracking velocimetry URL https://doi.org/10.4121/9b8b87d9-a099-480c-8f3b-0403acb114f9

[7] Taruffi F, Novais F and Viré A 2024 An experimental study on the aerodynamic loads of a floating offshore wind turbine under imposed motions *Wind Energy Science* **9** 343–358 URL https://doi.org/10.5194/wes-9-343-2024

[8] Lignarolo L, Ragni D, Krishnaswami C, Chen Q, Ferreira C S and Van Bussel G 2014 Experimental analysis of the wake of a horizontal-axis wind-turbine model *Renewable Energy* **70** 31–46 URL https://doi.org/10.1016/j.renene.2014.01.020

[9] Scarano F, Ghaemi S, Caridi G C A, Bosbach J, Dierksheide U and Sciacchitano A 2015 On the use of helium-filled soap bubbles for large-scale tomographic piv in wind tunnel experiments *Experiments in Fluids* **56** 42 URL https://doi.org/10.1007/s00348-015-1909-7

[10] Schneiders J F and Scarano F 2016 Dense velocity reconstruction from tomographic ptv with material derivatives *Experiments in fluids* **57** 139 URL https://doi.org/10.1007/s00348-016-2225-6

[11] Gambuzza S and Ganapathisubramani B 2023 The influence of free stream turbulence on the development of a wind turbine wake *Journal of Fluid Mechanics* **963** A19

[12] Messmer T, Peinke J, Croce A and Hölling M 2025 The role of motion-excited coherent structures in improved wake recovery of a floating wind turbine *Journal of Fluid Mechanics* **1018** A23

[13] Ivanell S, Mikkelsen R, Sørensen J N and Henningson D 2010 Stability analysis of the tip vortices of a wind turbine *Wind Energy* **13** 705–715